

Continuum description of profile scaling in nanostructure decay

Dionisio Margetis¹, Michael J. Aziz², and Howard A. Stone²

¹*Department of Mathematics, Massachusetts Institute of Technology, Cambridge, MA 02139*

²*Division of Engineering and Applied Sciences, Harvard University, Cambridge, MA 02138*

(Dated: May 29, 2003)

The relaxation of axisymmetric crystal surfaces with a single facet below the roughening transition is studied via a continuum approach that accounts for step energy g_1 and step-step interaction energy $g_3 > 0$. For diffusion-limited kinetics, free-boundary and boundary-layer theories are used for self-similar shapes close to the growing facet. For long times and $\frac{g_3}{g_1} < 1$, (a) a universal equation is derived for the shape profile, (b) the layer thickness varies as $(\frac{g_3}{g_1})^{1/3}$, (c) distinct solutions are found for different $\frac{g_3}{g_1}$, and (d) for conical shapes, the profile peak scales as $(\frac{g_3}{g_1})^{-1/6}$. These results compare favorably with kinetic simulations.

The drive toward smaller features in devices has fueled much interest in low-temperature kinetic processes such as growth, etching, and morphological relaxation. The constantly decreasing temperatures present increasing challenges for treatment of thermodynamics, kinetics and macroscopic evolution of surfaces. A crystal surface at equilibrium undergoes a roughening transition at a surface orientation-dependent temperature T_R [1, 2]. In equilibrium at temperature T , crystal facets (planar regions of the surface) have $T_R > T$, whereas orientations in continuously curved portions of the surface have $T_R < T$. In numerous nonequilibrium situations below T_R , a crystal surface relaxes to its equilibrium shape via the lateral motion of steps at a rate limited mainly by the diffusion of adatoms across terraces and attachment and detachment at step edges. Here we report a continuum treatment of this evolution using a partial differential equation (PDE) and obtain scaling laws and universal aspects of the solutions.

Morphological equilibration for surfaces above T_R is described by a continuum treatment [3, 4] where the surface free energy, which is an analytic function of the surface slope, and chemical potential [5] are ingredients in a fourth-order PDE for the evolution of the surface profile. However, this analysis is not applicable to surfaces below T_R because the surface free energy is not analytic in the surface orientation [2, 6, 7]; see Eq. (3) below.

Efforts to describe morphological evolution below T_R began in the mid 1980s and include simulations of the motion of monatomic crystalline steps and continuum thermodynamic approaches. In the latter, to account for evolution due to the motion of steps separating terraces below the basal plane's T_R , the step density, which is proportional to the surface slope, is introduced as a variable within a coarse-grained continuum description on a scale large compared to the step separation (typically, 1-10 nm). Expressions have been developed for the chemical potential of atoms at interacting step edges, leading to a nonlinear PDE for evolution of periodic sur-

face modulations [8, 9]; progress has been made toward solving the PDE [10, 11] but has been hindered when evolution involves facets [12, 13]. Kinetic simulations mimic nanoscale processes and so have been used to describe the detailed motion of many steps, as well as the evolution of facets, via coupled differential equations [14, 15, 16]. Nevertheless, the kinetic simulations are generally limited in their ability to characterize universal features of the shape evolution. Here we show that the shape profile, including the facet, can be treated using a continuum, thermodynamic description that illuminates scaling aspects of the kinetic behavior; for this purpose, we use an analytical framework that transcends the limitations of continuum approaches previously recognized [17].

Our analytical approach treats facet evolution as a free-boundary problem [12, 18]. The surface height is $h(\mathbf{r}, t)$, where $\mathbf{r} = (x, y) = r\mathbf{e}_r$ is the position vector in the plane of reference; see Fig. 1 for an axisymmetric shape. The step density is $|\nabla h|$; $\nabla h \equiv (h_x, h_y)$ and subscripts denote partial derivatives. Denoting the atomic volume by Ω and the surface current (atoms per length per time) by \mathbf{j} , the conservation equation for adatoms is

$$\frac{\partial h}{\partial t} + \Omega \nabla \cdot \mathbf{j} = 0. \quad (1)$$

The current is $\mathbf{j} = -c_s D_s \nabla \mu / k_B T$, where D_s and c_s are the surface diffusivity and adatom concentration, and $\mu(\mathbf{r})$ is the chemical potential of atoms at step edges; D_s is in principle a tensor function of ∇h .

We focus on diffusion-limited (DL) kinetics, where diffusion of adatoms across terraces is the rate-limiting process, and further assume that c_s is constant and D_s is a scalar constant. Equation (1) becomes

$$\frac{\partial h}{\partial t} = \frac{c_s D_s \Omega}{k_B T} \nabla^2 \mu. \quad (2)$$

Next, μ and h are related via the surface free energy per unit projected area, G . A common expression for G of vicinal surfaces for $T < T_R$ assumes that G depends on the step density according to [7, 11, 19]

$$G(\nabla h) = g_0 + g_1 |\nabla h| + \frac{1}{3} g_3 |\nabla h|^3. \quad (3)$$

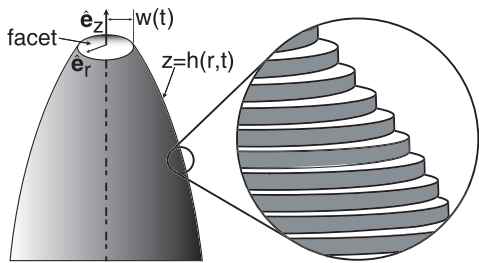


FIG. 1: View of an axisymmetric surface profile, on both the macroscale and the nanoscale where the atomic steps are evident. The evolution of surface morphology is caused by the motion of steps.

The g_0 term represents the surface free energy of the reference plane, g_1 is the step energy (line tension), and g_3 , which accounts for step-step interactions, includes entropic repulsions due to fluctuations at the step edges and pairwise energetic interactions between adjacent steps. All g_0, g_1 and g_3 are temperature dependent and we consider repulsive interactions between steps, $g_3 > 0$.

The surface chemical potential is derived from G by the relation [5, 7, 10] $\mu = -\Omega \nabla \cdot \frac{\delta G}{\delta(\nabla h)}$, where $\frac{\delta}{\delta(\nabla h)} \equiv \left(\frac{\partial}{\partial h_x}, \frac{\partial}{\partial h_y} \right)$ [20]:

$$\mu = -\Omega g_1 \nabla \cdot \left[\left(\frac{\nabla h}{|\nabla h|} \right) + \frac{g_3}{g_1} (|\nabla h| \nabla h) \right]. \quad (4)$$

The surface evolution equation follows by combination of Eqs. (1)–(4). We use cylindrical coordinates to describe the relaxation of axisymmetric shapes $h = h(r, t)$ that are smooth along the surface outside the facet and have negative slope, $\frac{\partial h}{\partial r} < 0$ (Fig. 1). Since $\nabla h = \mathbf{e}_r \frac{\partial h}{\partial r}$, it is convenient to define the dimensionless step density or surface slope $F(r, t) = -\frac{\partial h}{\partial r}$. The surface then evolves according to a fourth-order nonlinear PDE for F ,

$$\frac{\partial F}{\partial t} = \frac{3B}{r^4} - B \frac{g_3}{g_1} \frac{\partial}{\partial r} \nabla^2 \left[\frac{1}{r} \frac{\partial}{\partial r} (r F^2) \right]. \quad (5)$$

The material parameter $B = \frac{c_s D_s \Omega^2 g_1}{k_B T}$ has dimensions (length)⁴/time.

Equation (5) is supplemented with the initial condition $F(r, 0) = -H'(r)$, where $H(r) = h(r, 0)$ is the initial surface profile with the properties $H'(r) = 0$ for $r < W$ (the initial facet radius) and $H'(r) < 0$ for $r > W$. Also, there are four boundary conditions applied at the facet edge, $r = w(t)$. In particular, the height h and the current \mathbf{j} are continuous at the facet edge. The latter condition, along with $r\mathbf{j} \rightarrow \mathbf{0}$ as $r \rightarrow \infty$, ensures that the total mass is conserved. A consequence of Eq. (5) and the initial conditions is that no other facets are formed. Another condition is slope continuity at the facet edge, $F(w, t) = 0$ (i.e., local equilibrium [21, 22] and it is also consistent with kinetic simulations [14]). It is shown below that Eq. (5) furnishes $F(r, t) = O(\sqrt{r-w})$

as $r \rightarrow w^+$ where the coefficient is time dependent [23]. Finally, for $r \leq w$, where there is a facet, we extend continuously through Eqs. (1)–(4) the variable μ , although it no longer represents the true chemical potential, and the quantity $\mathbf{N} = \mathbf{e}_r N \equiv -\frac{\delta G}{\delta(\nabla h)}$ whose divergence yields μ/Ω [12, 24]. Hence the final two boundary conditions are continuity of μ and of \mathbf{N} . Although we now have a mathematically complete set of boundary conditions for Eq. (5), the issue of the boundary conditions remains a topic of discussion [25, 26]. Nevertheless, we expect that the main analytical and scaling ideas given below are independent of the detailed form of these conditions.

The boundary conditions described above relate $\frac{\partial F}{\partial t}$ to the derivatives of F^2 at $r = w^+$, the facet height $h_f(t)$ and the facet radius $w(t)$. By differentiating $h_f(t) = h(w^+(t), t)$ in time, we deduce that, at $r = w$,

$$B \left\{ 1 - \frac{g_3}{g_1} w [(F^2)' - 2w(F^2)'' - w^2(F^2)'''] \right\} = \dot{h}_f w^3, \quad (6)$$

where the dot denotes the time derivative. Then, an examination of μ and \mathbf{N} and their continuous extensions on the facet gives two more conditions at $r = w$ [24]:

$$w [3(F^2)' - w^2(F^2)'''] = 3 \frac{g_1}{g_3} = w [3(F^2)' - w(F^2)'']. \quad (7)$$

We now treat Eq. (5) with conditions (6) and (7) and $F = 0$ at the facet edge as a free-boundary problem [12]: there is a moving facet for $r < w(t)$, where $F = 0$, and this facet connects smoothly to the rest of the profile for $r > w(t)$. Note that this problem statement is valid for arbitrary $\frac{g_3}{g_1}$. In general, there exist an “outer” region, where only the line-tension energy g_1 is important, and an “inner” region in the neighborhood of the facet edge, where the step-step interaction energy g_3 becomes significant. Motivated by kinetic simulations with $\frac{g_3}{g_1} < 1$ [14], we set $\epsilon \equiv \frac{g_3}{g_1}$ and treat Eq. (5) analytically for the case with small ϵ , i.e., weak repulsive interactions. Because the small parameter ϵ multiplies the highest-order spatial derivative in Eq. (5), the shape evolution can be treated with boundary-layer theory [27]. We start with the solution for $\epsilon = 0$ where the corresponding facet radius $w(t; \epsilon)$ is denoted $w(t; 0) = w_0(t)$. From Eq. (5), the zeroth-order outer solution $F(r, t; 0) \equiv F_0(r, t)$ satisfies $\partial F_0 / \partial t = 3B/r^4$, which is integrated subject to the initial condition $F_0(r, 0) = -H'(r)$ to give

$$F_0(r, t) = 3Bt r^{-4} - H'(r), \quad r > w_0(t). \quad (8)$$

At the facet edge, $F_0(w_0, t) = 3Bt/w_0^4 - H'(w_0) \neq 0$, so the slope profile is discontinuous; this feature motivates a singular perturbation analysis.

The next step is to examine how the inclusion of a nonzero ϵ renders the slope continuous by retaining the highest derivative in Eq. (5). We therefore consider a region of width $\delta(t; \epsilon) \ll w$ in the neighborhood of the moving facet edge, and describe the solution in this region in

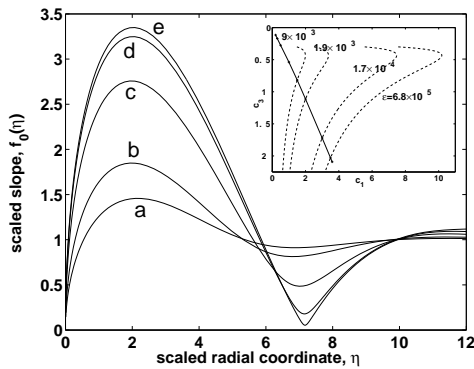


FIG. 2: Numerical solutions of Eq. (11) with the boundary conditions $f_0(0) = 0$ and $f_0(\infty) = 1$. Curves a-e are parametrized by $(c_1, c_3) = (1.5, -0.8183548), (2, -1.113031), (3, -1.72107502), (3.5, -2.0302102), (3.6, -2.09232155)$ and correspond to $\epsilon = 9.2 \times 10^{-3}, 1.9 \times 10^{-3}, 1.7 \times 10^{-4}, 6.8 \times 10^{-5}, 5.7 \times 10^{-5}$. Inset: The dashed curves are described by Eq. (13) for a conical initial shape and different ϵ , while the solid curve shows c_3 as a function of c_1 from the numerical solutions of Eq. (11).

terms of the local variable $\eta \equiv (r - w)/\delta$. Thus, we seek a long-time similarity solution that depends on the distance from the facet edge and time, $F(r, t; \epsilon) = \mathcal{F}(\eta, t; \epsilon)$. We anticipate that, to leading order in ϵ ,

$$\mathcal{F}(\eta, t) \sim a_0(t)f_0(\eta; \epsilon), \quad \eta = [r - w(t; \epsilon)]/\delta(t; \epsilon), \quad (9)$$

where f_0 depends implicitly on ϵ through the boundary conditions. Substitution of (9) into (5) and balance of the leading-order terms in ϵ gives

$$\frac{\dot{w}\delta^3}{B\epsilon a_0}f_0' = (f_0'')'''' + O\left(\frac{\delta}{w}, \frac{\delta^4}{\epsilon w^4}, \frac{\dot{\delta}\delta^3}{\epsilon B}\right). \quad (10)$$

Thus, $\frac{\dot{w}\delta^3}{B\epsilon a_0}$ must be time-independent and we take it equal to unity without affecting observable quantities such as F or w . It follows that $\delta(t; \epsilon) = O(\epsilon^{1/3})$, independent of the (axisymmetric) initial conditions, which is a prediction for a scaling law for the boundary-layer width in the case of DL kinetics. The neglected terms in Eq. (10) are $O(\epsilon^{1/3}) \ll 1$. Furthermore, the leading-order facet radius is $w(t)^4 \sim 4B \int_0^t dt' \tilde{w}(t')^3 a_0(t)$, where $\tilde{w} = \frac{w}{\Delta}$ and $\Delta(t) \equiv \epsilon^{-1/3} \delta(t; \epsilon)$.

We next examine solutions of Eq. (10) along with the prescribed boundary conditions. First, this equation is integrated once via matching $\mathcal{F}(\eta, t)$ with the outer solution (8), i.e., taking $\eta \gg 1$ and $r \rightarrow w^+$ simultaneously. We find $a_0(t) = 3Btw^{-4} - H'(w)$, which by Eq. (9) determines the explicit time dependence of the surface slope. Because at this point we have imposed no restrictions other than axisymmetry on the initial shape, we have in fact obtained a universal equation for $f_0(\eta)$, i.e.,

$$(f_0'')'''' = f_0 - 1, \quad (11)$$

which is to be solved with $f_0(0) = 0$ and $f_0(\eta \rightarrow \infty) = 1$. Near the origin, $f_0(\eta)$ has the behavior

$$f_0(\eta) \sim c_1\eta^{1/2} + c_3\eta^{3/2} + c_5\eta^{5/2} + c_6\eta^3 + \dots, \quad (12)$$

where all coefficients c_n with $n \geq 5$ are known in terms of c_1 and c_3 . Equation (11) has a growing mode for $\eta \gg 1$, which must be suppressed in order to satisfy the condition at ∞ ; thus, c_3 is found numerically in terms of c_1 . We solve Eq. (11) numerically and so obtain a family of similarity solutions $f_0(\eta)$ for different values of c_1 [28]; see Fig. 2. We next show how the solution $f_0(\eta)$ depends on ϵ , which requires imposing conditions such as (7).

The substitution of Eq. (9) into Eq. (7) and use of the relations $(f_0'')'_{\eta=0} = c_1^2$ and $(f_0'')''_{\eta} = 4c_1c_3$ from Eq. (12) yield two parametric equations for c_1 and c_3 . In the case with a conical initial shape, discussed at length below, continuity of the variable μ implies [24]

$$(c_1c_3)\epsilon^{1/3} = -\frac{3}{4^{5/3}}[c_3^{-2}(c_3^2 - \frac{1}{16})^2(c_3^2 + \frac{3}{16})^{-1}]^{1/3}. \quad (13)$$

The intersection of the curve (13) with the set of points (c_1, c_3) that result from numerically solving Eq. (11) is shown in the inset of Fig. 2, and determines a value of ϵ for each of the solution curves of the main part of the figure. Thus, we have determined a family of ϵ -dependent similarity solutions $f_0(\eta; \epsilon)$.

There is one more scaling law that comes from the analysis. Each of the curves $f_0(\eta)$ in Fig. 2 has a well-defined absolute maximum. Using (12) each maximum may be estimated to be $O(c_1^{3/2}|c_3|^{-1/2})$ and to occur at $\eta_{max} = O(c_1/|c_3|)$, which is independent of ϵ to leading order. Thus, according to Eq. (13), c_1 and c_3 are $O(\epsilon^{-1/6})$ and so the maximum slope is predicted to be $O(\epsilon^{-1/6})$.

We now compare the predictions from this continuum approach based on Eq. (5) with the kinetic simulations for the DL case reported by Israeli and Kandel [14] for a conical initial shape. In their simulations these authors vary a parameter, $g = (\text{const.}) \cdot g_3$, holding g_1 fixed, which in our analysis is equivalent to changing ϵ . Their simulations furnished a g -dependent family of solutions (see their Figs. 4(b) and 6), which correspond to our ϵ -dependent curves $f_0(\eta; \epsilon)$. Israeli and Kandel also derived a complicated, g -dependent differential equation in the scaling variable $x = r/(Bt)^{1/4}$ (not to be confused with the cartesian coordinate), which, in the limit of small g , effectively reduces to our (11). However, on the basis of their equation they found multiple solutions whereas we provide a unique solution $f_0(\eta; \epsilon)$ for each ϵ .

Next, we consider scaling behavior with ϵ . First, we examine the scaling of the boundary layer near the facet edge. We define the boundary-layer thickness as the distance from the facet edge, x_0 , to the position of the peak, x_{peak} , of the step density, F_{peak} . In Fig. 3 we show the results of kinetic simulations (symbols) for $x_{\text{peak}} - x_0$ vs. g and compare with our $\epsilon^{1/3}$ scaling prediction (solid line). Second, in Fig. 3 we examine how F_{peak} varies with

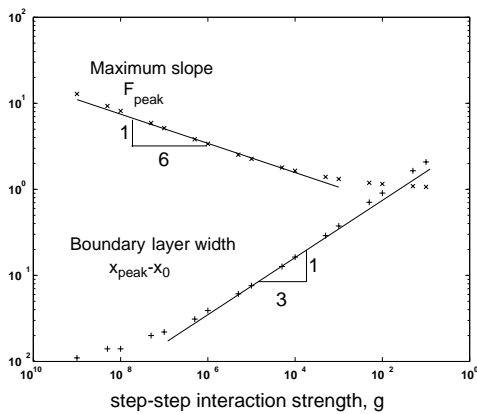


FIG. 3: Log-log plot of the boundary-layer thickness $\delta(t; \epsilon)$ and the maximum of step density F_{peak} as functions of ϵ . The crosses represent the results of kinetic simulations given to us by Israeli and Kandel [14] for the DL case. Here, $\delta(t; \epsilon)$ is estimated as the distance $x_{\text{peak}} - x_0$ between the facet edge, $x_0 = w(Bt)^{-1/4}$, where $F = 0$, and the position x_{peak} of the maximum of F . The straight lines correspond to the $\epsilon^{1/3}$ and $\epsilon^{-1/6}$ scaling laws predicted according to Eq. (10).

g , for which the results of kinetic simulations (symbols) are compared with the $\epsilon^{-1/6}$ scaling prediction (solid line). In both cases the agreement is very good. With regard to the deviations in the boundary-layer width for $g < 10^{-6}$, as ϵ decreases in the simulations x_{peak} approaches the facet edge so that the boundary-layer width is relatively small on the scale of the step spacing and is consequently poorly defined; its evaluation in discrete simulations thus becomes prone to errors.

As shown above, qualitative predictions, such as the form of the multiple solution curves, and quantitative predictions, such as the $\epsilon^{1/3}$ scaling of the boundary-layer width and the $\epsilon^{-1/6}$ scaling of the maximum of the slope, can be deduced from a continuum approach based on Eq. (5) with the use of free-boundary and boundary-layer theories [29]. Further, simple analytical arguments show that, for any admissible initial slope $F(r, 0) = \kappa r^\nu$, for a wide range of ν including $-4 < \nu \leq 1$, the facet radius is $w = O(t^{1/(\nu+4)})$ at sufficiently long times. In addition, we expect that, for a class of non-axisymmetric initial shapes, the near-facet boundary layer width still retains the $O(\epsilon^{1/3})$ scaling for the isotropic surface free energy of Eq. (3).

The continuum approach and the free-boundary viewpoint capture the essential physics of crystal surface evolution below T_R . This development should give further impetus to continuum approaches to morphological evolution even at the nanoscale for structures far below T_R .

This research was supported by the Harvard NSEC. We thank M. Z. Bazant and R. R. Rosales for useful discussions, and also thank N. Israeli and D. Kandel for

valuable feedback and for sharing with us details of their simulation results.

-
- [1] W. K. Burton and N. Cabrera, *Discuss. Faraday Soc.* **5**, 33 (1949).
 - [2] M. Wortis, in *Fundamental Problems in Statistical Mechanics VI*, edited by E. G. D. Cohen (North-Holland, Amsterdam, 1985), pp. 87–123.
 - [3] W. W. Mullins, *J. Appl. Phys.* **28**, 333 (1957).
 - [4] W. W. Mullins, *J. Appl. Phys.* **30**, 77 (1959).
 - [5] C. Herring, in *Physics of Powder Metallurgy*, edited by W. E. Kingston (McGraw-Hill, NY, 1951).
 - [6] C. Herring, *Phys. Rev.* **82**, 87 (1951).
 - [7] E. E. Gruber and W. W. Mullins, *J. Phys. Chem. Solids* **28**, 875 (1967).
 - [8] A. Rettori and J. Villain, *J. Phys. (France)* **49**, 257 (1988).
 - [9] F. Lancon and J. Villain, in *Kinetics of Ordering and Growth at Surfaces*, edited by M. Lagally (Plenum, New York, 1990).
 - [10] M. Ozdemir and A. Zangwill, *Phys. Rev. B* **42**, 5013 (1990).
 - [11] H.-C. Jeong and E. D. Williams, *Surf. Sci. Reports* **34**, 171 (1999).
 - [12] H. Spohn, *J. Phys. I France* **3**, 69 (1993).
 - [13] V. B. Shenoy and L. B. Freund, *J. Mech. Phys. Solids* **50**, 1817 (2002).
 - [14] N. Israeli and D. Kandel, *Phys. Rev. B* **60**, 5946 (1999).
 - [15] N. Israeli, H.-C. Jeong, D. Kandel, and J.D. Weeks, *Phys. Rev. B* **61**, 5698 (2000).
 - [16] N. Israeli and D. Kandel, *Phys. Rev. B* **62**, 13707 (2000).
 - [17] N. Israeli and D. Kandel, *Phys. Rev. Lett.* **88**, 116103 (2002).
 - [18] J. Hager and H. Spohn, *Surf. Sci.* **324**, 365 (1995).
 - [19] C. Jayaprakash, C. Rottman, and W. F. Saam, *Phys. Rev. B* **30**, 6549 (1984).
 - [20] Therefore, $\mu = -\Omega \left[\frac{\partial}{\partial x} \frac{\partial G}{\partial h_x} + \frac{\partial}{\partial y} \frac{\partial G}{\partial h_y} \right]$.
 - [21] C. Jayaprakash, W. F. Saam, and S. Teitel, *Phys. Rev. Lett.* **50**, 2017 (1983).
 - [22] H.P. Bonzel, *Prog. Surf. Sci.* **67**, 45 (2001).
 - [23] According to [21], the behavior $O(\sqrt{r-w})$ at equilibrium reflects a Pokrovsky-Talapov phase transition in the surface free energy.
 - [24] D. Margetis, M. J. Aziz, and H. A. Stone, to be published.
 - [25] A. Chame, S. Rousset, H.P. Bonzel, and J. Villain, *Bulg. Chem. Commun.* **29**, 398 (1996).
 - [26] Our boundary conditions appear to be consistent with the global variational approach taken by [13].
 - [27] E.J. Hinch, *Perturbation Methods* (Cambridge University Press, Cambridge, 1991), Ch. 5.
 - [28] We solve Eq. (11) numerically by integrating from $\eta_0 \ll 1$ towards $\eta^* \gg 1$ for fixed c_1 to satisfy $f_0(\eta^*) = 1$. This procedure yields a family of similarity solutions $f_0(\eta)$ corresponding to a curve $c_3(c_1)$ where $c_1 > 0$ and $c_3 < 0$.
 - [29] This approach contrasts with the smoothing of the surface free energy, e.g. in M. V. R. Murty, *Phys. Rev. B* **62**, 17004 (2000).